Received May 30, 2021, accepted June 11, 2021, date of publication June 15, 2021, date of current version June 22, 2021.

Digital Object Identifier 10.1109/ACCESS.2021.3089589

Theoretical and Experimental Study of Floating Foundation Vibration Reduction System Based on Deep Neural Network

ZHU LONGJI, WENLIUHAN HEISHA, AND ZOU SHUANG
Earthquake Engineering Research and Test Center, Guangzhou University, Guagnzhou 510000, China
Corresponding author: Wenliuhan Heisha (1111716013@e.gzhu.edu.cn)

ABSTRACT A floating foundation vibration reduction system with an air spring as a vibration isolation element has been widely used in the foundation of large ultra-precision instruments. With the excellent vibration isolation performance of the air spring, its complex dynamic nonlinear behavior is always a research difficulty. In this paper, a dynamic model of a floating foundation vibration reduction system based on the restoring force of air spring is derived. The structure of the recurrent convolution neural network (RCNN) is proposed based on combining the working characteristics of a convolution neural network and a long short-term memory neural network, and the dynamic model of a floating foundation vibration reduction system is established with the restoring force of the air spring calculated by the RCNN as the input. Finally, a test experiment was designed to compare the dynamic characteristics of the traditional numerical model and three deep neural network models in the floating foundation. The results show that convolution neural network, long short-term memory, and RCNN models could predict the vibration response of floating foundation vibration reduction system, and the RCNN model had better performance for a floating foundation.

INDEX TERMS Floating foundation, dynamic nonlinear model, air spring, recurrent convolution neural network.

I. INTRODUCTION

A floating foundation vibration reduction system (hereinafter referred to as a floating foundation) is an efficient vibration reduction technology, which is often used in the field of precision instruments vibration reduction [1], [2]. A floating foundation consists of an instrument foundation and vibration reduction elements. The vibration reduction elements are mainly composed of a steel spring with a viscous damper [3] or an air spring with auxiliary chamber (hereinafter referred to as an air spring) [4], as shown in Fig. 1. Compared with a steel spring, an air spring has lower stiffness, and thus it can better meet the vibration reduction requirements of large ultra-precision instruments in the low-frequency micro vibration stage.

With the expansion of floating foundations in applications and the complex and changeable working environment, the accuracy of the dynamic nonlinear model of air springs is required to be increasingly higher for floating foundation dynamic analysis. However, the stiffness and damping of air springs have highly nonlinear characteristics, which is always the difficulty in the study of an air spring constitutive model.

In the numerical modeling of an air spring, scholars decompose it into different components, such as a rubber air bag (main chamber) and a throttle device (orifice) connecting a main chamber and an auxiliary chamber [5], [6]. Two aspects should be considered in the modeling of an air spring rubber airbag (main chamber): one is the stiffness caused by the air pressure in the airbag [7], and the other is the stiffness and damping caused by rubber deformation [8]. Two aspects should be considered while modeling the orifice: one part is the stiffness of the high-speed airflow caused by the air pressure difference between the two air chambers while passing through the orifice, and the other part is the friction damping and inertia damping of air in the orifice [9].

In an experimental study on a semi-automobile air suspension system, Zargar and Bahram [10] pointed out that damping in the air spring will increase nonlinearly as the

The associate editor coordinating the review of this manuscript and approving it for publication was Wenbing Zhao.

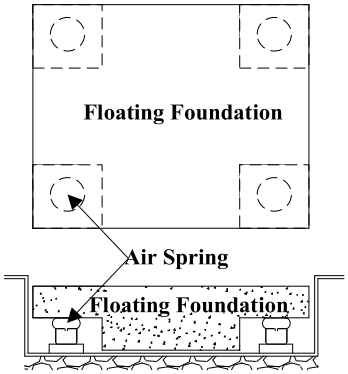

FIGURE 1. Structural diagram of a floating foundation vibration reduction system.

natural frequency of the system increases, especially in the 4 to 6 Hz region. Suda *et al.* [11] established an air spring suspension system model using A'GEM software and arrived at a conclusion similar to that of Zargar. To investigate the air suspension of high-speed trains, Docquier *et al.* [12] compared and analyzed five air spring models and presented air spring models that would be suitable below 8 Hz and above 8 Hz. Porumamilla *et al.* [13] further studied the characteristics of the displacement transmission rate of air springs, pointing out the variable frequency damping characteristics of air springs and highlighting that the natural frequency changes with the opening of the orifice. It can be observed from the aforementioned literature that the air spring model is related to the frequency and amplitude of the excitation.

The existing models ignore or simplify the nonlinear characteristics of the air spring [14], which are the Helmholtz resonance generated by the high-speed air flow in the gas chamber [4] and the congestion of the gas in the throttle device [15]. Moreover, the numerical model weakens the coupling relationship between the interactions of each unit, which leads to a big difference between the air spring model and the actual measurement results in the nonlinear stage.

In recent years, deep neural networks have been widely used in the field of mechanical modeling and have shown great potential for highly nonlinear dynamic behavior simulation, for example, a convolutional neural network (CNN) [16] with the ability to extract data features and a long short-term memory (LSTM) [17] network with good performance in time sequencing. Combined with the characteristics of the above two neural networks, recurrent convolution neural network (RCNN) has good performance for both feature extraction and time sequencing [18]. Wang *et al.* [19] proposed a new prognostics framework, named RCNN, for remaining useful life prediction of machinery. Experimental results show that the proposed RCNN has a clear advantage in accuracy and convergence compared with some existing CNN-based prognostics approaches and other typical machine learning models. Li *et al.* [20] used an LSTM to model unsteady aerodynamics and aeroelasticity of the multiple Mach numbers for wings, and LSTM has a good simulation capability for unsteady and nonlinear aerodynamic models caused by high-speed airflow. Li *et al.* [21] proposed an improved neural network based on LSTM to simulate the flutter model of long-span bridge panels, and they verified the effectiveness of the neural network through the designed wind tunnel experiment. Zhang *et al.* [22] compared the full sequence input data and the stacked input data to train the LSTM and verified that the stacked input data could train the LSTM more effectively by comparing the numerical model analysis results and the earthquake response prediction of a 3-story building. Chen *et al.* [23] combined CNN and Bayesian estimation and proposed a new Naïve Bayes CNN (NB-CNN) with an identification rate of 99.9% for cracks. Oh *et al.* [24] took ground motion (GM) as input and the structural response as output, and they used a CNN for training. Their model was proved to be effective in predicting the seismic response of reinforced concrete structures by a shaking table experiment. Kim *et al.* [25] successfully predicted the maximum response of a building structure by using a CNN to extract the features in the restoring force model of the building and the important features of the input structure, soil, and GM. In another paper, Oh *et al.* [26] designed four kinds of artificial neural networks based on the average period, predominant period, duration, and the acceleration peak value of input GM combined with the input resonance area, the sum of resonance area, and the sum of modal weighted resonance area. Eshkevari *et al.* [27] proposed a dynamic neural network model (DynNet) to predict the response of multi-degree-of-freedom systems. The model tested two different four degrees of freedom shear structures: one with plastic stiffness, the other with third-order nonlinear elastic stiffness. It showed that the network can predict the time history including displacement, velocity, acceleration, and internal force.

Given the increasing application of air springs, it is difficult for the existing constitutive models derived from numerical equations to simulate the highly nonlinear behavior of air springs, and thus it is urgent to establish a reliable dynamic nonlinear model under the natural state. The deep neural network model can capture the characteristics of highly nonlinear dynamic behavior caused by high-speed airflow in the air spring chamber as well as the coupling effect of different mechanical elements. In this paper, the vibration test of a floating foundation with different frequencies and amplitudes is designed, and then an RCNN is designed according to the characteristics of the vibration test data of the floating foundation vibration reduction system, and the RCNN model of air spring's restoring force is trained. The performance of the CNN, LSTM and RCNN models was compared by training experimental data. The results show that the CNN, LSTM and RCNN models could predict the vibration response of floating foundation vibration reduction system, and the RCNN neural network had a higher prediction accuracy for the vibration response of a floating foundation.

This paper is organized as follows: Section 2 introduces a numerical model of an air spring and a dynamic model of a floating foundation vibration reduction system

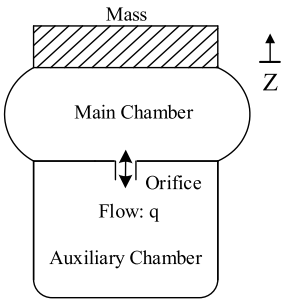

FIGURE 2. Structure diagram of an air spring.

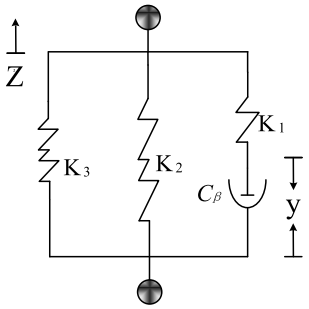

FIGURE 3. Numerical model of the air spring.

based on which the restoring force of the air spring is derived. Section 3 introduces the proposed RCNN architecture for the restoring force of the air spring and prediction. Section 4 introduces the algorithm of the numerical model and deep neural network model. In section 5, the proposed methodology is validated by comparing the dynamic response of floating foundation calculated by the numerical model with the predictions of the RCNN, LSTM, and CNN models based on experimental data. Finally, Section 6 discusses the limitations of the proposed approach and summarizes the conclusions of this paper.

II. DYNAMIC MODEL OF THE FLOATING FOUNDATION VIBRATION REDUCTION SYSTEM

A. AIR SPRING MODEL

The numerical model of the air spring assumes that each element of its structure is an independent mechanical model, the material is isotropic, and the internal air satisfies the thermodynamic properties under an ideal state. Then, the momentum conservation of the mass on the spring, the gas volume equation of the main and auxiliary chambers, the mass flow equation of the orifice, and the mass continuity equation of the orifice are derived. Finally, the numerical model is simplified into series and parallel linear springs/linear or nonlinear damping elements. The structure of an air spring is shown in Fig. 2.

The numerical model is expressed as follows [28]:

$$F_a = K_1(z - y) + (K_2 + K_3)z \tag{1}$$

and

$$C_\beta \dot{y}^\beta = K_1(z - y) \tag{2}$$

where,

$$K_1 = \frac{\kappa\lambda A A_V P_0}{V_A}; \quad K_2 = \frac{1-\lambda}{\lambda}K_1; \; K_3 = (P_0 - P_{at})A_z$$

$$C_\beta = \lambda A R_\beta(\lambda\rho_0 A_V)^\beta; \quad \lambda = \frac{V_B}{V_A + V_B}$$

Here, F_a is the force of the air spring; K_1 and C_β are the stiffness and damping of the orifice, respectively; K_3 is the main chamber stiffness; K_2 is the auxiliary chamber stiffness; A is the effective area of the main chamber at the equilibrium position; A_z is the change rate of the effective area calculated by dA/dz; A_v is the volume change rate of the main chamber; V_A is the volume of the auxiliary chamber; V_B is the volume of the auxiliary chamber; F_a is the restoring force of the air spring; P_0 is the initial pressure; P_{at} is the atmospheric pressure; y is the gas displacement in the orifice; ρ_0 is the initial gas density; R_β is the damping coefficient; z is the vertical displacement calculated from the equilibrium position; and β damping optimization coefficient. The numerical model of the air spring is shown in Fig. 3.

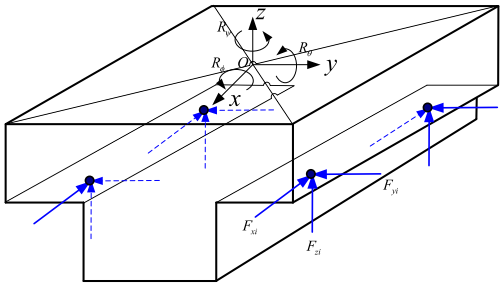

FIGURE 4. The computing diagram of the dynamic model of the floating foundation.

B. DYNAMIC MODEL OF THE FLOATING FOUNDATION VIBRATION REDUCTION SYSTEM

To unify the numerical modeling and the deep neural network modeling, the dynamic model of the floating foundation is established by taking the time history restoring force of the air spring under the external excitation as the dynamic input. The computing diagram is shown in Fig. 4.

Suppose that the floating foundation is a rigid body. According to the Euler angle definition, the transformation from a floating foundation coordinate system to a ground coordinate system can be realized by three consecutive rotations around different coordinate axes. Therefore, the coordinate system of the floating foundation supported by multiple air springs can be transformed into a ground coordinate system by rotating three times around the z-axis, y-axis, and x-axis of the floating foundation as follows:

$$R_\psi = \begin{bmatrix} cos\,\psi & -sin\,\psi & 0 \\ sin\,\psi & cos\,\psi & 0 \\ 0 & 0 & 1 \end{bmatrix}, R_\theta = \begin{bmatrix} cos\,\theta & 0 & sin\,\theta \\ 0 & 1 & 0 \\ -sin\,\theta & 0 & cos\,\theta \end{bmatrix},$$

and

$$R_\phi = \begin{bmatrix} 1 & 0 & 0 \\ 0 & cos\,\phi & -sin\,\phi \\ 0 & sin\,\phi & cos\,\phi \end{bmatrix}.$$

Here, R_ψ, R_θ. and R_ϕ are the rotation angles around the z-axis, y-axis, and x-axis, respectively. The floating foundation can be transformed into a ground coordinate as follows:

$$R = \begin{bmatrix} cos\,\theta\,cos\,\psi & sin\,\phi\,sin\,\theta\,cos\,\psi - cos\,\phi\,sin\,\psi & cos\,\phi\,sin\,\theta\,cos\,\psi + sin\,\phi\,sin\,\psi \\ cos\,\theta\,sin\,\psi & sin\,\phi\,sin\,\theta\,sin\,\psi + cos\,\phi\,cos\,\psi & cos\,\phi\,sin\,\theta\,sin\,\psi - sin\,\phi\,cos\,\psi \\ -sin\,\theta & sin\,\phi\,cos\,\theta & cos\,\phi\,cos\,\theta \end{bmatrix} \quad (3)$$

According to Newton's second law, the acceleration in each direction is obtained by

$$\begin{bmatrix} \ddot{x} \\ \ddot{y} \\ \ddot{z} \end{bmatrix} = \begin{bmatrix} \frac{\sum F_{xi}}{m} \\ \frac{\sum F_{yi}}{m} \\ \frac{\sum F_{zi}}{m} \end{bmatrix} \times R \quad (4)$$

Here, m is the mass of the floating foundation; F_{xi}, F_{yi}, and F_{zi} are the components in the x-, y-, and z-directions of the i-th restoring force, respectively; $\ddot{x}$, $\ddot{y}$, and $\ddot{z}$ represent the acceleration of the floating foundation in the x-, y-, and z-directions, respectively. The moment of the air spring force to the center of mass of the floating foundation can be expressed as

$$M = \begin{bmatrix} M_x \\ M_y \\ M_z \end{bmatrix} = \begin{bmatrix} \sum F_{xi}L_{xi} \\ \sum F_{yi}L_{yi} \\ \sum F_{zi}L_{zi} \end{bmatrix} \quad (5)$$

Here, L_{xi}, L_{yi}, and L_{zi} are the distances of the i-th restoring force from the origin of the floating foundation coordinate system in the x-, y-, and z-directions. According to the Euler angle transformation matrix, the transformation between the air spring force and the angular velocity of the floating foundation can be obtained. This paper studies the micro-vibration of the floating foundation, and thus, in the above matrix, the sine equals 0 and cosine equals 1, which can be simplified as follows:

$$\begin{bmatrix} p \\ q \\ r \end{bmatrix} = \begin{bmatrix} 1 & 0 & -sin\theta \\ 0 & cos\,\phi & sin\,\phi\,cos\,\theta \\ 0 & -sin\,\phi & cos\,\phi\,cos\,\theta \end{bmatrix} \begin{bmatrix} \dot{\phi} \\ \dot{\theta} \\ \dot{\psi} \end{bmatrix} \approx \begin{bmatrix} \dot{\phi} \\ \dot{\theta} \\ \dot{\psi} \end{bmatrix} \quad (6)$$

The angular velocity of the floating foundation can be obtained by the calculation method of the moment of momentum as follows:

$$\begin{bmatrix} \ddot{\phi} \\ \ddot{\theta} \\ \ddot{\psi} \end{bmatrix} = \begin{bmatrix} \frac{\sum F_{xi}L_{xi} + (I_x - I_z)\,\dot{\theta}\dot{\psi}}{I_x} \\ \frac{\sum F_{yi}L_{yi} + (I_z - I_x)\dot{\phi}\dot{\psi}}{I_y} \\ \frac{\sum F_{zi}L_{zi} + (I_x - I_y)\dot{\phi}\dot{\theta}}{I_z} \end{bmatrix} \quad (7)$$

Here, I_x, I_y, and I_z are the cross-sectional moments of inertia of the x-axis, y-axis, and z-axis, respectively. Then, the acceleration of the floating foundation in three directions is as follows (8), as shown at the bottom of the next page:

III. DEEP NEURAL NETWORK MODEL OF AN AIR SPRING

A. RECURRENT CONVOLUTION NEURAL NETWORK

Convolutional neural network (CNN) has a good performance in data feature extraction, which can clean the input data and enhance the feature density of the input data. At the same time, another important characteristic of a CNN is its translation invariance. For earthquakes, a CNN can extract features [25] (such as the GM parameter) in the vibration wave, and the feature is independent of the position in the wave. However, a CNN lacks memory when processing time sequence data, which means that each information is input into the network as an independent individual and the network does not know the state of the previous information. Long short-term memory network (LSTM) adds a method that can transmit information at multiple time steps. The information in each time sequence segment can be recorded and transmitted, and the information transferred can be updated according to the update of the time sequence to save and transmit the important information (data features) in the past.

In the dynamic analysis of an air spring, the actual situation is that the excitation of a vibration wave to the air spring is in order. When the air spring encounters a strong amplitude excitation in the vibration wave, the system will enter (or temporarily enter) a nonlinear state, and thus the stiffness and damping of the air spring will show nonlinear characteristics in the subsequent vibration excitation. Therefore, in the process of maintaining the stiffness and damping information, the air spring system will be updated with the change of vibration excitation.

The RCNN proposed in this paper is an artificial neural network that combines the characteristics of a CNN for data feature extraction and LSTM for time-sequence processing. This neural network extracts the hidden information (data features) of input data from CNN layers, transfers the data features with higher quality and concentration to the LSTM layer, then uses the function of storing and forgetting information of LSTM to process the sequence relationship of time sequence, and finally makes the network prediction and the characteristics of input data highly mapped in the time dimension. At the same time, a CNN can remove redundant

data and reduce the amount of computation because it has abstract feature ability. The RCNN is calculated as follows:

A feature chain with time series attribute is obtained by a convolution layer of the ground vibration acceleration as follows:

$$x_t = f\left(\ddot{x}_g \otimes W + b\right) \tag{9}$$

where x_t is the extracted eigenvalue, $\ddot{x}_g$ is the input data (ground vibration acceleration); $\otimes$ is the convolution operation; W is the weight parameter; b is the bias; and $f(\cdot)$ is the activation function. The time-dependent feature chain (9) is introduced into the LSTM neural network as follows:

The forgetting gate:

$$f_t = \sigma(x_t W_x^f + h_{t-1} W_h^f) \tag{10}$$

The input gate:

$$i_t = \sigma(x_t W_x^i + h_{t-1} W_h^i) \tag{11}$$

and

$$\tilde{C}_t = tanh(x_t W_x^c + h_{t-1} W_h^c) \tag{12}$$

The output gate:

$$o_t = \sigma(x_t W_x^o + h_{t-1} W_h^o) \tag{13}$$

The memory unit:

$$C_t = \sigma(f_t \times C_{t-1} + i_t \times \tilde{C}_t) \tag{14}$$

The output unit:

$$h_t = tanh(C_t) \times o_t \tag{15}$$

Finally, the full connection layer is connected with the target data to calculate the loss value and feedforward. The RCNN structure is shown in Fig. 5.

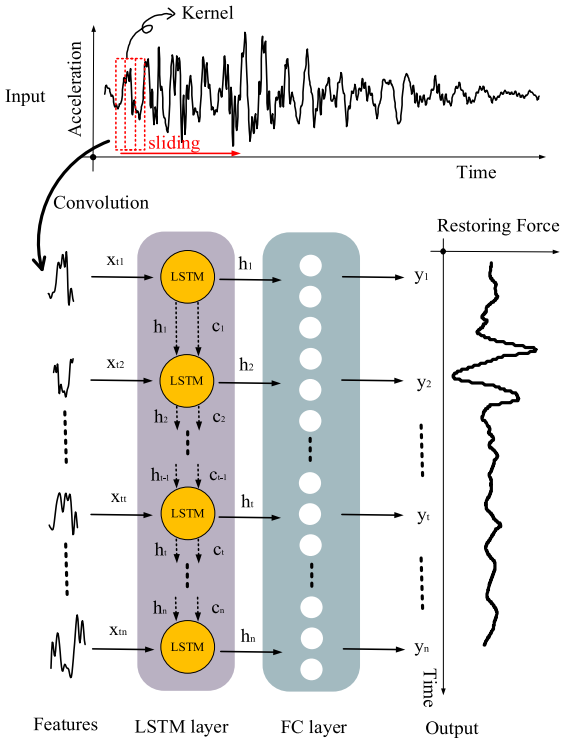

FIGURE 5. Recurrent convolution neural network structure.

B. RECURRENT CONVOLUTION NEURAL NETWORK MODEL OF AN AIR SPRING

The structure of the RCNN proposed in this paper is as follows:

(1) Input data

The basic unit of input data is a $1 \times \boldsymbol{x_t}$ dimensional vector ($\boldsymbol{x_t}$ represents the total steps of the excitation wave), and each vector represents a vibration acceleration time history excitation wave. The input data is a combination of multiple vectors ($\boldsymbol{x_1}$, $\boldsymbol{x_2}$.....$\boldsymbol{x_{l-1}}$, $\boldsymbol{x_l}$) $\times$ $\boldsymbol{x_t}$ dimension

$$\begin{bmatrix} \ddot{x} \\ \ddot{y} \\ \ddot{z} \end{bmatrix} = \begin{bmatrix} \dfrac{\sum F_{xi}\left(\cos\theta\cos\psi\cos\theta\,\sin\psi - \sin\theta\right)}{m} + \dfrac{\sum\left(F_{zi} + (I_x - I_y)\dot{\phi}\dot{\theta}/L_{zi}\right)}{2I_z} \\ \dfrac{\sum F_{yi}\left[\sin\phi\,\sin\theta\,(\cos\psi + \sin\psi) - \cos\phi\,(\sin\psi - \cos\psi)\right]}{m} \\ \dfrac{\sum F_{zi}\left[\cos\phi\,\sin\theta\,(\cos\psi + \sin\psi) + \sin\phi\,(\sin\psi - \cos\psi) + \cos\phi\,\cos\theta\right]}{m} \end{bmatrix} \begin{bmatrix} 0 \\ +\dfrac{\sum F_{yi}\sin\phi\,\cos\theta}{m} + \dfrac{\sum\left(F_{zi} + \dfrac{(I_x - I_y)\,\dot{\phi}\dot{\theta}}{L_{zi}}\right)}{2I_z} \\ +\dfrac{\sum\left(F_{xi} + \dfrac{(I_x - I_z)\,\dot{\theta}\dot{\psi}}{L_{xi}}\right)}{I_x} + \dfrac{\sum\left(F_{yi} + \dfrac{(I_z - I_x)\,\dot{\phi}\dot{\psi}}{L_{yi}}\right)}{I_y} \end{bmatrix} \tag{8}$$

Algorithm 1 Numerical Model of the Floating Foundation Vibration Reduction System

Input: $\ddot{x}_g$, K_1, K_2, K_3, C_β, c, β, tolerance
for (i=0; i<step-1;i++)
{$pz = z_i + \dot{z}_i\Delta t + \left(\frac{1}{2} - \beta\right)\ddot{z}_i\Delta t^2$
$f'\left(y_{(n+1)}\right) = \frac{\beta C_\beta}{\Delta t}\left(\frac{y_{(n+1)} - y_{(n)}}{\Delta t}\right)^{\beta-1} + K_1$
if abs $(f'\left(y_{(n+1)}\right))$ > tolerance
$y^{new}_{(n+1)} = y^{old}_{(n+1)} - \frac{f\left(y_{(n+1)}\right)}{f'\left(y_{(n+1)}\right)}$
else $y^{new}_{(n+1)} = y^{old}_{(n+1)}$
y= $y^{new}_{(n+1)}$
$pz = z_{i+1}$
Calculation of the restoring force of the air spring:
$F_i = K_1(pz - y) + (K_2 + K_3)pz$
Calculation of dynamic response of floating foundation:
$\ddot{z} = \frac{\sum F_{zi}[cos\ \phi sin\ \theta(cos\ \psi + sin\ \psi) + sin\ \phi(sin\ \psi - cos\ \psi) + cos\ \phi cos\ \theta]}{m} + \frac{\sum\left(F_{xi} + \frac{(I_x - I_z)\dot{\theta}\dot{\psi}}{L_{xi}}\right)}{I_x} + \frac{\sum\left(F_{yi} + \frac{(I_z - I_x)\dot{\phi}\dot{\psi}}{L_{yi}}\right)}{I_y}$
Return $\ddot{z}_i, \dot{z}_i, z_i$

vector ($\boldsymbol{x_l}$ represents the number of samples of the excitation wave), and $\boldsymbol{x_t}$ and $\boldsymbol{x_l}$ change according to the input data.

(2) Convolution layer

The convolution kernel of each layer is (1,3) and has 32 filters. There is one pooling layer, and the maximum pooling calculation is used.

(3) LSTM layer

The model uses two layers of the LSTM structure, and each layer contains 30 units.

(4) Full connection layer

There are two layers of the full connective layer with 30 neurons in each layer.

In this study, the deep neural network model training environment was as follows: Windows Server 2019, Anaconda 3, Python 3.7, TensorFlow 2.2, Keras 2.4.2, CPU E5-2609, and GPU GTX TITAN.

IV. ALGORITHMS OF THE DYNAMIC MODEL OF A FLOATING FOUNDATION VIBRATION REDUCTION SYSTEM

In this study, only the vertical motion was considered. The numerical model calculation was programmed in C++ language, and deep neural network model calculation was programmed in Python language. The two algorithms are given below.

V. EXPERIMENTAL VERIFICATION

A. PARAMETERS OF THE FLOATING FOUNDATION VIBRATION REDUCTION SYSTEM

The physical parameters of the air spring are given in Table 1, and the physical parameters of the floating foundation vibration reduction system are given in Table 2.

Algorithm 2 Deep Neural Network Model of the Floating Foundation Vibration Reduction System

Train model
Input: batch_size = 10, Adam (lr=0.001, decay=0.0001), epochs = 50000
Input data $\mathbf{X}_t \times \mathbf{X}_l$, Target data $\mathbf{y}_t$
Scaler data to [−1,1]: Scaler_$\mathbf{X}_t \times \mathbf{X}_l$, Scaler_$\mathbf{y}_t$
Deep neural network model:
model.add(Conv1D(filters=32, kernel_size=3, activation='relu'), input_shape= ($\mathbf{X}_t \times \mathbf{X}_l$))
model.add(Conv1D(filters=32, kernel_size=3, activation='relu', dropout(0.5)))
model.add(MaxPooling1D(pool_size=2))
model.add(Flatten())
model.add(LSTM(30, return_sequences=True, stateful=False), Activation('relu'))
model.add(LSTM(30, return_sequences=True, stateful=False), Activation('relu'))
model.add(Dense(30), Activation('relu'))
model.add(Dense(30), Activation('relu'))
model.add(Dense(1))
model.compile(loss='categorical_crossentropy', optimizer='adam', metrics=['accuracy'])
separate $\mathbf{X}_t \times \mathbf{X}_l$ and $\mathbf{y}_t$ into training data and test data: X_train, y_train, X_test, y_test
model.fit(X_train, y_train, batch_size=batch_size, validation_data=(X_test, y_test))
model.save
Prediction restoring force of the air spring:
model_best = load_model
Input data $\mathbf{X}_t^p$ for predict
$\mathbf{y}_t^p$ = model_best.predict ($\mathbf{X}_t^p$)
$F_i = \mathbf{y}_t^p$
Calculation of dynamic response of floating foundation:
$\ddot{z} = \frac{\sum F_{zi}[cos\ \phi\ sin\ \theta(cos\ \psi + sin\ \psi) + sin\ \phi(sin\ \psi - cos\ \psi) + cos\ \phi\ cos\ \theta]}{m} + \frac{\sum\left(F_{xi} + \frac{(I_x - I_z)\dot{\theta}\dot{\psi}}{L_{xi}}\right)}{I_x} + \frac{\sum\left(F_{yi} + \frac{(I_z - I_x)\dot{\phi}\dot{\psi}}{L_{yi}}\right)}{I_y}$
Return $\ddot{z}_i, \dot{z}_i, z_i$

TABLE 1. Physical parameters of the air spring.

Parameter	Value
Effective area	0.4185 m^2
Rate of change rate in the effective area	0.248 m
Rate of change in the volume of the main chamber	0.284 m^2
Initial air pressure	658 KPa
Initial gas density	7.5 kg/m^3
Initial volume of the main chamber	0.103 m^3
Initial volume of the auxiliary chamber	0.35 m^3
Variable index	1.4
Damping coefficient	1.42 × 106 $N/m^2(s/kg)^\beta$
$\boldsymbol{\beta}$	1.65

B. EXPERIMENTAL TRAINING DATA SET

The test equipment used included the ENDEVCO 86 constant current source accelerometer from the United States,

TABLE 2. Physical parameters of the floating foundation vibration reduction system.

Parameter	Value
Floating foundation quality	239 t
Size	$8 \times 11 \times 3$ m^3
Number of air springs	12
Vertical design frequency	0.8 Hz
Horizontal design frequency	0.8 Hz

TABLE 3. Vibration test conditions.

Number	Vibration test conditions
Project 1	Environmental vibration as the vibration source
Project 2	Electric drill as the vibration source
Project 3	The low-frequency vibration as the vibration source from the vibrator
Project 4	The low-frequency vibration as the vibration source from the vibrator
Project 5	The medium-frequency vibration as the vibration source from the vibrator
Project 6	The medium-frequency vibration as the vibration source from the vibrator
Project 7	The high-frequency vibration as the vibration source from the vibrator
Project 8	The high-frequency vibration as the vibration source from the vibrator

B&K6 channel vibration and acoustic input module equipment from Denmark, B&K vibration analysis software PULSE OMA from Denmark, several signal transmission wires, and a Sony notebook computer. Two measuring points (A and B) were arranged in the positive center of the upper platform of the floating foundation and the ground beside the floating foundation. Each measuring point had three accelerometers to measure the vibration acceleration in the horizontal and vertical directions. At the same time, the internal air pressure time history data of the air spring was output through the air spring pressure stabilizing system, and the restoring force of air spring was calculated according to the following formula:

$$F_a = (P_A - P_{at})\, A_e \tag{16}$$

where F_a is the restoring force of air spring; P_A is the air pressure of main chamber of air spring; P_{at} is the standard atmospheric pressure; and A_e is the effective area.

As shown in Table 3, vibration tests were carried out at a certain distance from the floating foundation under eight test conditions using the vibrator as the excitation source for sampling. The test site is shown in Fig. 6.

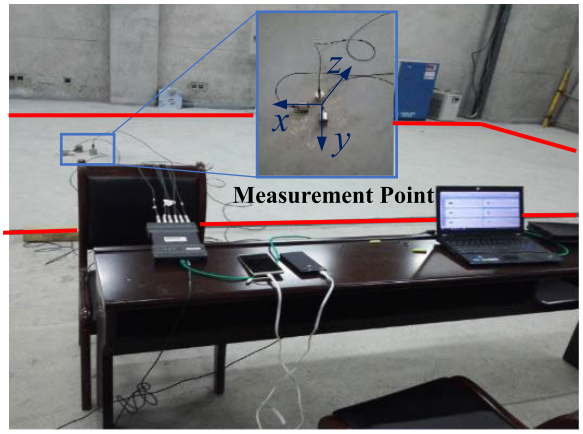

FIGURE 6. Vibration test site of the floating foundation vibration reduction system, where the red line is the outline of the floating foundation.

C. DATA PREPROCESSING

The 40 ground motions (GMs) recorded in the vibration test and their corresponding air spring pressure time histories were divided into five categories. The first category and the second category were environmental vibration and electric drill vibration, respectively; the third to fifth categories were low frequency vibration, medium frequency vibration, and high frequency vibration respectively. These GMs and their corresponding air spring pressure time histories were preprocessed by normalization. Five GMs were selected from each of the five categories of vibration test data, and a total of 25 GMs were selected as the input and the corresponding air spring pressure time history as the target output. These 25 samples were used as training sample sets. The other three GMs in the first and second categories and two GMs from the third to the fifth categories were selected as the input and the corresponding air spring pressure time history as the target output. These 12 samples were used as validation sample sets. Finally, the remaining GMs from the third to the fifth categories were used as the input, and the corresponding air spring pressure time history was used as the output validation. These three samples were used as the prediction sets, and the low frequency (Sample 1), medium frequency (Sample 2), and high frequency (Sample 3) were used as the sample labels, respectively. Table 4 shows the details of the RCNN.

D. NUMERICAL MODEL AND DEEP NEURAL NETWORK MODELS OF THE FLOATING FOUNDATION

The floating foundation vibration reduction system was modeled and analyzed, which was based on the numerical model of the air spring and deep neural network models (including the CNN, LSTM, and RCNN models, and the details are shown in Table 5) trained with the experimental data sets.

Figure 7 shows the dynamic response of the floating foundation obtained by four simulation analysis models. Fig. 8 shows the error rate of peak acceleration (PA) between

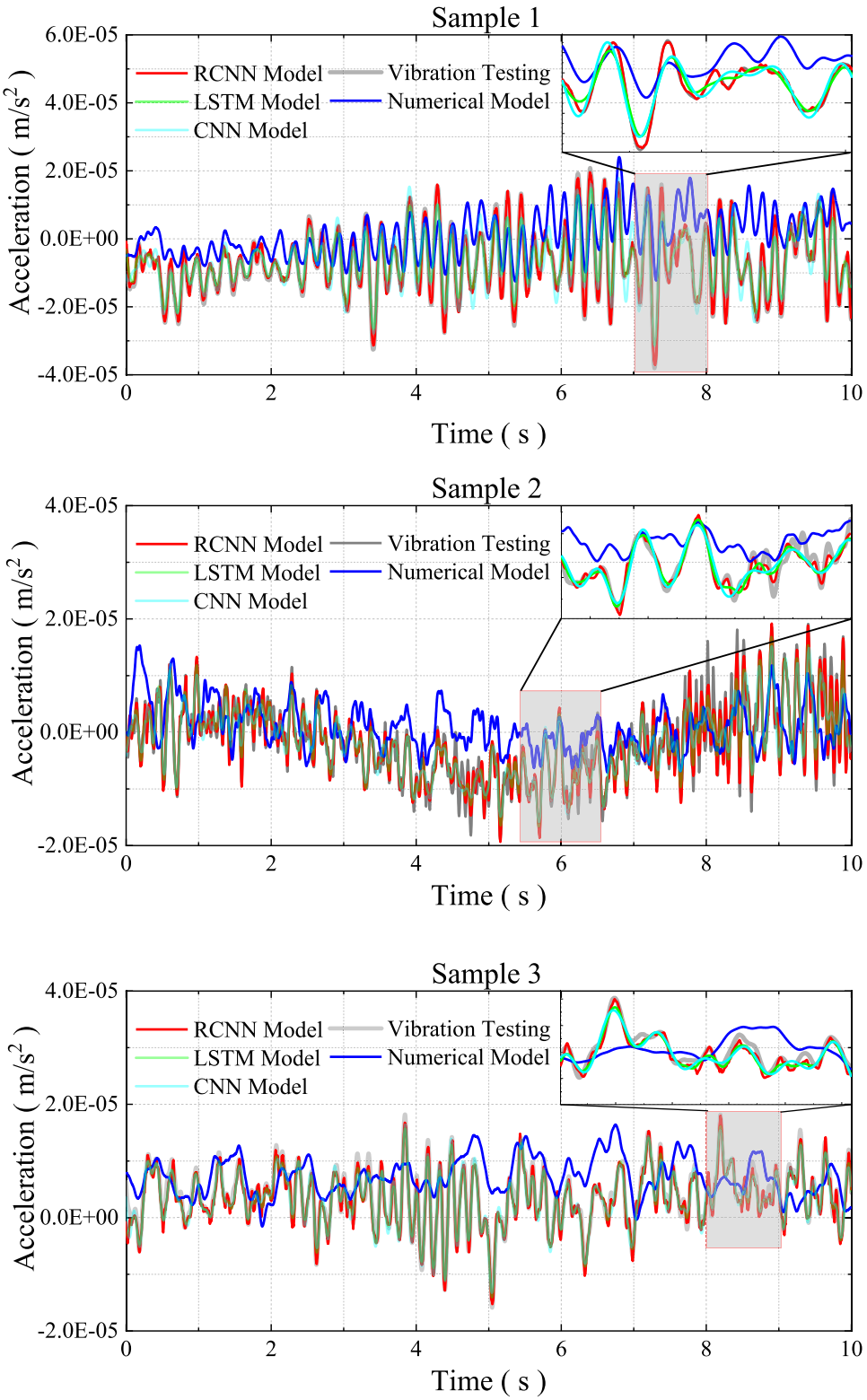

FIGURE 7. Comparison of the calculation results between the numerical model and the deep neural network models.

the test results and the calculated results of the four models. The error distribution is shown in Fig. 9. To better illustrate the prediction error, the probability density function (PDF) of the normalized error distribution π_i is defined as

$$\pi_i = PDF\left\{\frac{y_i^{ture} - y_i^{pred}}{max\left(\left|y_i^{ture}\right|\right)}\right\} \tag{17}$$

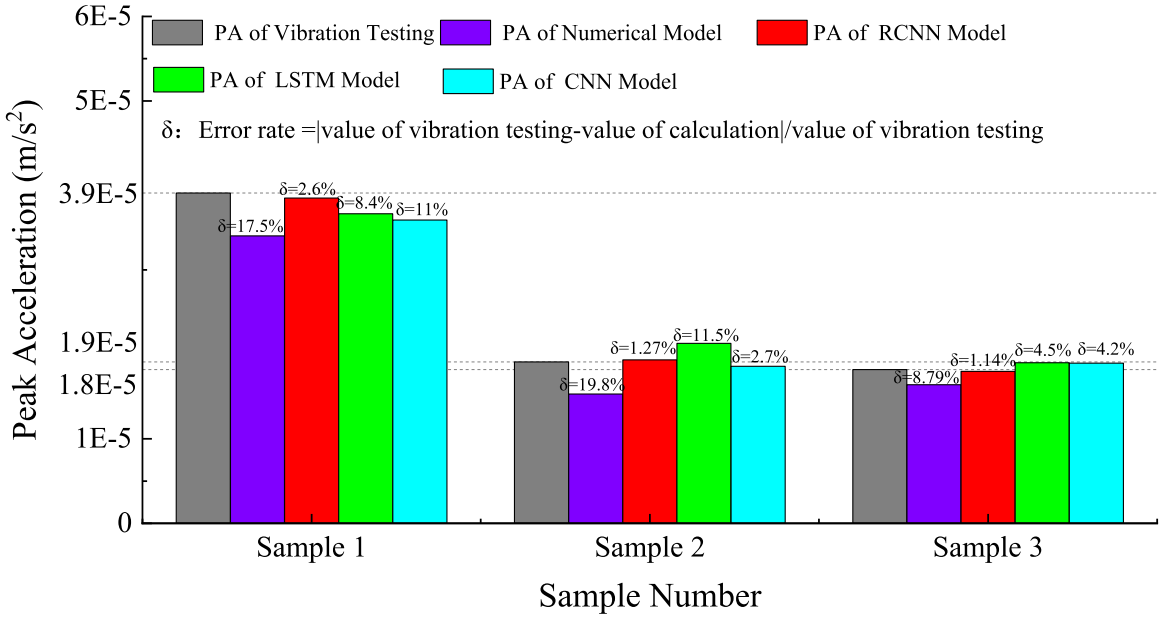

FIGURE 8. Peak acceleration error rate between the numerical model and the deep neural network models' calculation.

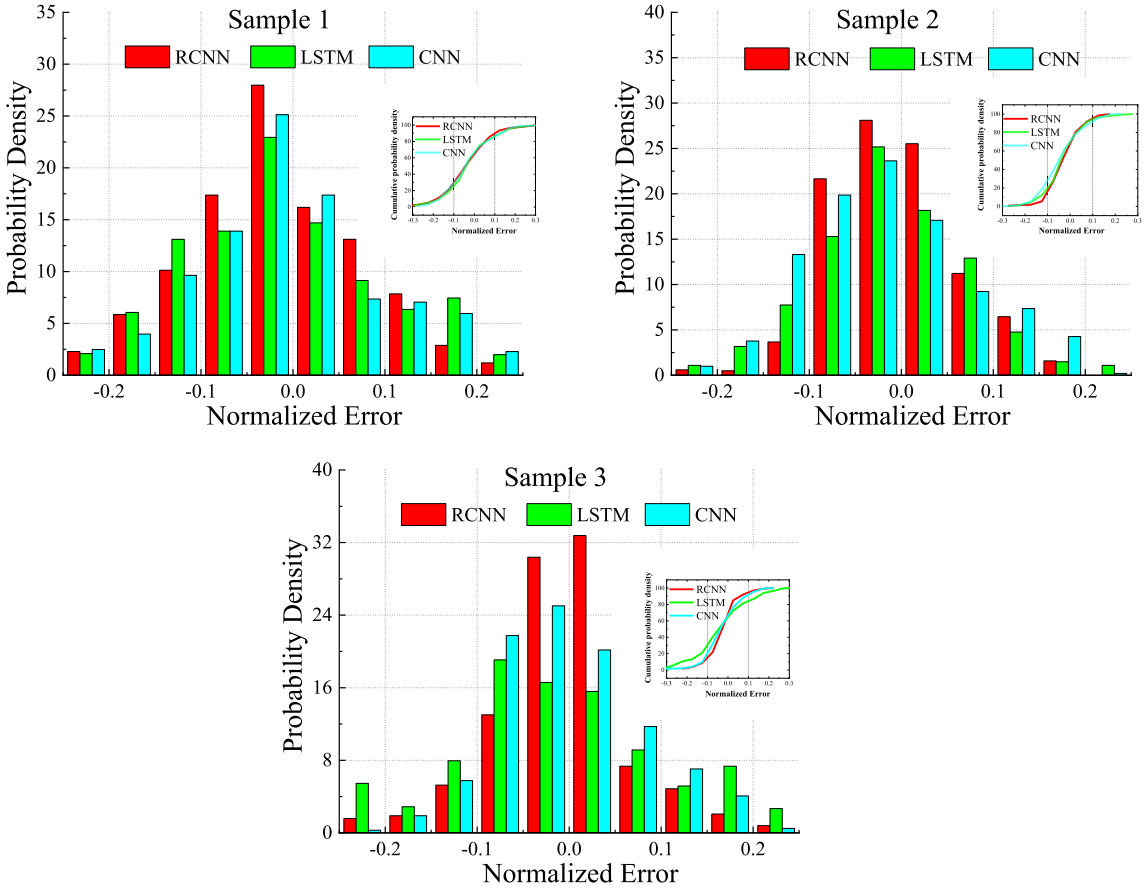

FIGURE 9. Error distribution of the prediction for the samples in the deep neural network models.

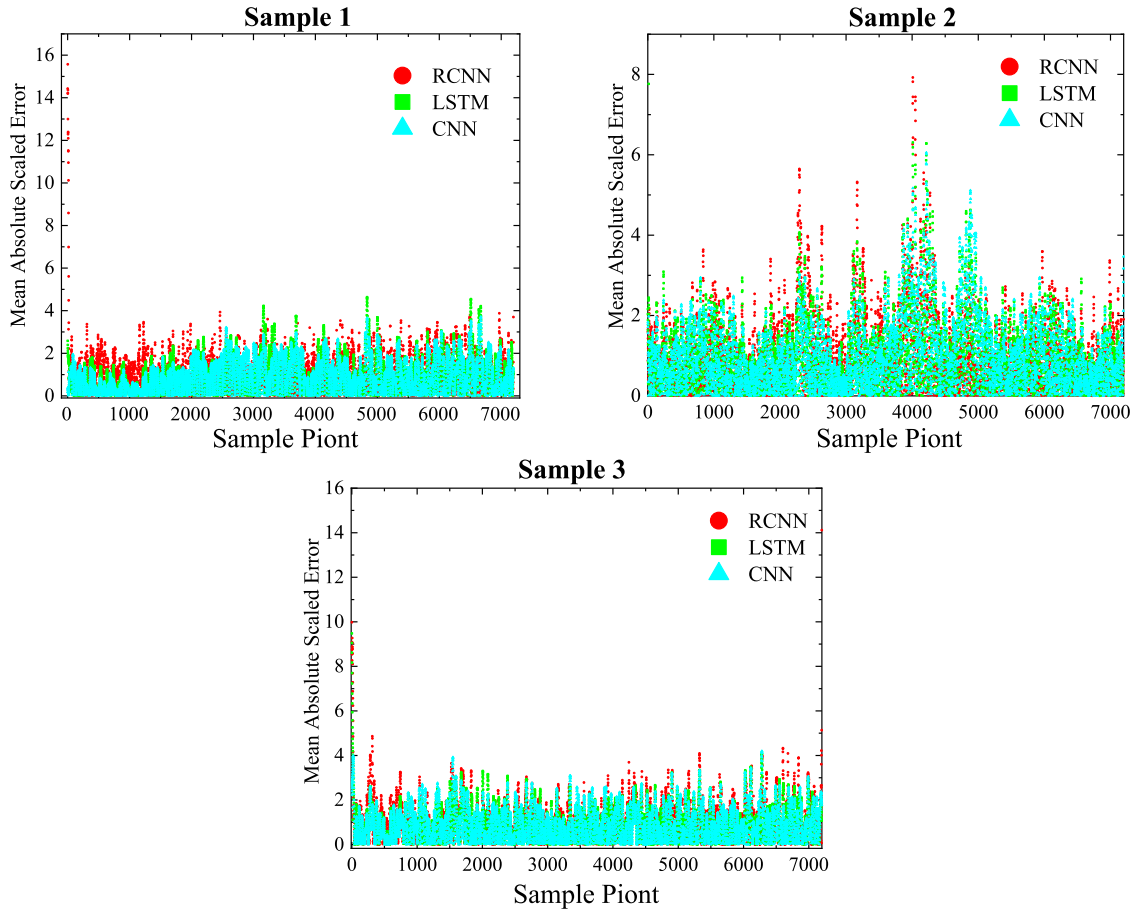

FIGURE 10. The MASE for the predictions on the samples.

TABLE 4. Configuration of RCNN.

Parameter	Value
The size of input vector for training model	7680×25
Filter size	32
Pooling size	2
Kernel size	3
Activation function	ReLu
Learning rate	0.001
Weight decay	0.0001
The probability of dropout	0.5
Number of layers	7
Epochs	50000

TABLE 5. Details of deep neural network models.

Models	RCNN	LSTM	CNN
Epochs	50000	50000	50000
Number of parameters	39,927	36,961	43,141
Number of layers	7	6	6
Number of training data sets	25	25	25
Number of validation data sets	12	12	12
Number of prediction sets	3	3	3
Sample length	7680	7680	7680
Sample labels	Sample 1 Sample 2 Sample 3	Sample 1 Sample 2 Sample 3	Sample 1 Sample 2 Sample 3

Besides, the mean absolute scaled error (MASE) is defined as

$$MASE = \left| \frac{\hat{\varepsilon}_{i,t}^2}{\frac{1}{T}\sum_{t=2}^{T} |y_t - y_{t-1}|} \right| \tag{18}$$

where $\hat{\varepsilon}_{i,t}^2$ is the mean squared error. The MASE is shown in Fig. 10.

Figure 7 and Fig. 8 compare the acceleration time history and PA of the floating foundation between the calculated values of the numerical model and the deep neural network (RCNN, LSTM, and CNN) models and the experimentally

measured values. As shown, the predicted values of deep neural network models were very close to the experimental values, and the minimum error of PA was only 1.14% in RCNN, 4.5% in LSTM, and 2.7% in CNN. Compared with the experimentally measured value, the minimum error of the calculated value of the numerical model was 8.79%. Figure 9 is the probability density distribution of the error between the calculated value of the deep neural network models and the experimentally measured value. As shown, more than 90% of the errors in Sample 1 and Sample 3 were concentrated in the range of −10% to 10%, and more than 80% of the errors in Sample 2 were concentrated in the range of −10% to 10%. Compared with LSTM and CNN, the error of RCNN was more concentrated in the range of −10% to 10% in the three samples. Figure 10 shows the MASE between the calculated value of the deep neural network models and the experimentally measured value. The MASE distribution of the sample points of Sample 1 and Sample 3 was relatively uniform, and the sample points of 2500 to 4500 in Sample 2 had relatively large error values. The main reason for the large error of Sample 2 in Fig. 9 and Fig. 10 was that there is a large baseline drift in the vibration test of the floating foundation, and thus there was a lot of noise interference. Based on the above analysis, compared with the numerical model, the deep neural network models could more accurately simulate the test results of the floating foundation, and the RCNN model had higher prediction accuracy for the experimental data.

VI. CONCLUSION

Based on the working characteristics of a CNN and an LSTM neural network, an RCNN structure was established to train the restoring force model of an air spring isolator. Taking the restoring force of the air spring as the input of the floating foundation, a dynamic model of the floating foundation is derived. The main contributions of this work can be summarized as follows:

(1) The dynamic model of the floating foundation based on the restoring force of the air spring was derived.

(2) According to the correlation between the vibration frequency and mechanical model of the air spring, a vibration test of the floating foundation was designed, and a dynamic model of the floating foundation was constructed based on the test data as the training data set.

(3) The predicted results of the recurrent convolution neural network were very close to the actual vibration test results. Compared with LSTM and CNN, the error of RCNN was more concentrated in the range of − 10% to 10% in the three samples. The MASE distribution of Sample 1 and Sample 3 was relatively uniform, while the MASE of Sample 2 was larger at the sample points of 2500 to 4500.

This paper validates the feasibility of RCNN for predicting the dynamic characteristics of a floating foundation vibration reduction system. In the future, more accurate experiments will be designed to obtain a general constitutive model of an air spring in a natural state and use it in structural dynamic analysis and prediction to completely replace traditional numerical modeling.

REFERENCES

[1] A. Soueid, H. Amick, and T. Zsirai, "Addressing the environmental challenges of the NIST advanced measurement laboratory," *Proc. SPIE*, vol. 5933, Aug. 2005, Art. no. 59330N.

[2] M. Arif, M. S. Dewey, G. L. Greene, and W. M. Snow, "Facilities for fundamental neutron physics research at the NIST cold neutron research facility," *J. Res. Nat. Inst. Standards Technol.*, vol. 98, no. 1, p. 135, Jan. 1993.

[3] M. Çahin, "3-D analytical treatment of base isolation for mechanical testing systems," *Gazi Univ. J. Sci. A, Eng. Innov.* vol. 5, no. 1, pp. 1–15, 2018.

[4] B. Voigtländer, P. Coenen, V. Cherepanov, P. Borgens, T. Duden, and F. S. Tautz, "Low vibration laboratory with a single-stage vibration isolation for microscopy applications," *Rev. Sci. Instrum.*, vol. 88, no. 2, Feb. 2017, Art. no. 023703.

[5] M. Berg, "A model for rubber springs in the dynamic analysis of rail vehicles," *Proc. Inst. Mech. Eng., F, J. Rail Rapid Transit*, vol. 211, no. 2, pp. 95–108, Mar. 1997.

[6] M. Berg, "A non-linear rubber spring model for rail vehicle dynamics analysis," *Vehicle Syst. Dyn.*, vol. 30, nos. 3–4, pp. 197–212, Sep. 1998.

[7] J.-H. Moon and B.-G. Lee, "Modeling and sensitivity analysis of a pneumatic vibration isolation system with two air chambers," *Mech. Mach. Theory*, vol. 45, no. 12, pp. 1828–1850, Dec. 2010.

[8] M. Berg, "A three—Dimensional airspring model with friction and orifice damping," *Vehicle Syst. Dyn.* vol. 33, no. 1, pp. 528–539, 1999.

[9] N. Docquier, P. Fisette, and H. Jeanmart, "Multiphysic modelling of railway vehicles equipped with pneumatic suspensions," *Vehicle Syst. Dyn.*, vol. 45, no. 6, pp. 505–524, Jun. 2007.

[10] B. Zargar, "Model development, validation and nonlinear control of pneumatic suspensions," Ph.D. dissertation, Dept. Mech. Eng., Univ. Ottawa, Ottawa, ON, Canada, 2007.

[11] Y. Suda and S. Kumaki, "Study on curving characteristic of vehicles with non linear air suspension," *JSME Int. J. C*, vol. 41, no. 3, pp. 668–673, 1998.

[12] N. Docquier, P. Fisette, and H. Jeanmart, "Model-based evaluation of railway pneumatic suspensions," *Vehicle Syst. Dyn.*, vol. 46, no. 1, pp. 481–493, Sep. 2008.

[13] H. Porumamilla, A. G. Kelkar, and J. M. Vogel, "Modeling and verification of an innovative active pneumatic vibration isolation system," *J. Dyn. Syst., Meas., Control*, vol. 130, no. 3, pp. 031001-1–031001-12, May 2008.

[14] N. Oda and S. Nishimura, "Vibration of air suspension bogies and their design," *Bull. JSME*, vol. 13, no. 55, pp. 43–50, 1970.

[15] M. Li, "Mechanism analysis on dynamic characteristics of air spring system with auxiliary chamber," Ph.D. dissertation, Dept. Traffic Eng., Jiangsu Univ., Zhenjiang, China, 2012.

[16] A. Krizhevsky, I. Sutskever, and G. E. Hinton, "ImageNet classification with deep convolutional neural networks," *Commun. ACM*, vol. 60, no. 6, pp. 84–90, May 2017.

[17] F. Gers, "Long short-term memory in recurrent neural networks," Ph.D. dissertation, School Math. Phys., Univ. Hannove, Hanover, Germany, Verlag nicht ermittelbar, 2001.

[18] H. Peng, J. Li, S. Wang, L. Wang, Q. Gong, R. Yang, B. Li, P. S. Yu, and L. He, "Hierarchical taxonomy-aware and attentional graph capsule RCNNs for large-scale multi-label text classification," *IEEE Trans. Knowl. Data Eng.*, vol. 33, no. 6, pp. 2505–2519, Jun. 2021.

[19] B. Wang, Y. Lei, T. Yan, N. Li, and L. Guo, "Recurrent convolutional neural network: A new framework for remaining useful life prediction of machinery," *Neurocomputing*, vol. 379, pp. 117–129, Feb. 2020.

[20] K. Li, J. Kou, and W. Zhang, "Deep neural network for unsteady aerodynamic and aeroelastic modeling across multiple mach numbers," *Nonlinear Dyn.*, vol. 96, no. 3, pp. 2157–2177, May 2019.

[21] W. Li, S. Laima, X. Jin, W. Yuan, and H. Li, "A novel long short-term memory neural-network-based self-excited force model of limit cycle oscillations of nonlinear flutter for various aerodynamic configurations," *Nonlinear Dyn.*, vol. 100, no. 3, pp. 2071–2087, 2020.

[22] R. Zhang, Z. Chen, S. Chen, J. Zheng, O. Büyüköztürk, and H. Sun, "Deep long short-term memory networks for nonlinear structural seismic response prediction," *Comput. Struct.*, vol. 220, pp. 55–68, Aug. 2019.

[23] F.-C. Chen and M. R. Jahanshahi, "NB-CNN: Deep learning-based crack detection using convolutional neural network and Naïve bayes data fusion," *IEEE Trans. Ind. Electron.*, vol. 65, no. 5, pp. 4392–4400, May 2018.
[24] B. K. Oh, Y. Park, and H. S. Park, "Seismic response prediction method for building structures using convolutional neural network," *Struct. Control Health Monit.*, vol. 27, no. 5, p. e2519, 2020.
[25] T. Kim, O.-S. Kwon, and J. Song, "Response prediction of nonlinear hysteretic systems by deep neural networks," *Neural Netw.*, vol. 111, pp. 1–10, Mar. 2019.
[26] B. K. Oh, B. Glisic, S. W. Park, and H. S. Park, "Neural network-based seismic response prediction model for building structures using artificial earthquakes," *J. Sound Vibrat.*, vol. 468, Mar. 2020, Art. no. 115109.
[27] S. S. Eshkevari, M. Takáč, S. N. Pakzad, and M. Jahani, "DynNet: Physics-based neural architecture design for linear and nonlinear structural response modeling and prediction," 2020, *arXiv:2007.01814*. [Online]. Available: https://arxiv.org/abs/2007.01814
[28] K. Shimozawa and T. Tohtake, "An air spring model with non-linear damping for vertical motion," *Quart. Rep. RTRI*, vol. 49, no. 4, pp. 209–214, 2008.

ZHU LONGJI was born in Jiangxi, China. He is currently pursuing the Ph.D. degree with the Earthquake Engineering Research and Test Center, Guangzhou University. His current research interests include vibration reduction and isolation of precision instruments and micro vibration isolation technology.

WENLIUHAN HEISHA was born in Xinjiang, China. He received the Ph.D. degree from Tohoku University. His current research interests include vibration reduction and isolation of precision instruments and micro vibration isolation technology.

ZOU SHUANG was born in Liaoning, China. She received the Ph.D. degree from Tohoku University. Her current research interests include vibration reduction and isolation of precision instruments and micro vibration isolation technology.